Chemical Physics Letters 850 (2024) 141460

Contents lists available at ScienceDirect

Chemical Physics Letters

journal homepage: www.elsevier.com/locate/cplett

Research paper

Accurate and efficient prediction of optical gaps in silicon and germanium nanoparticles using a high-local-exchange density functional

Corentin Villot, Ka Un Lao *

Department of Chemistry, Virginia Commonwealth University, Richmond, VA 23284, USA

GRAPHICAL ABSTRACT

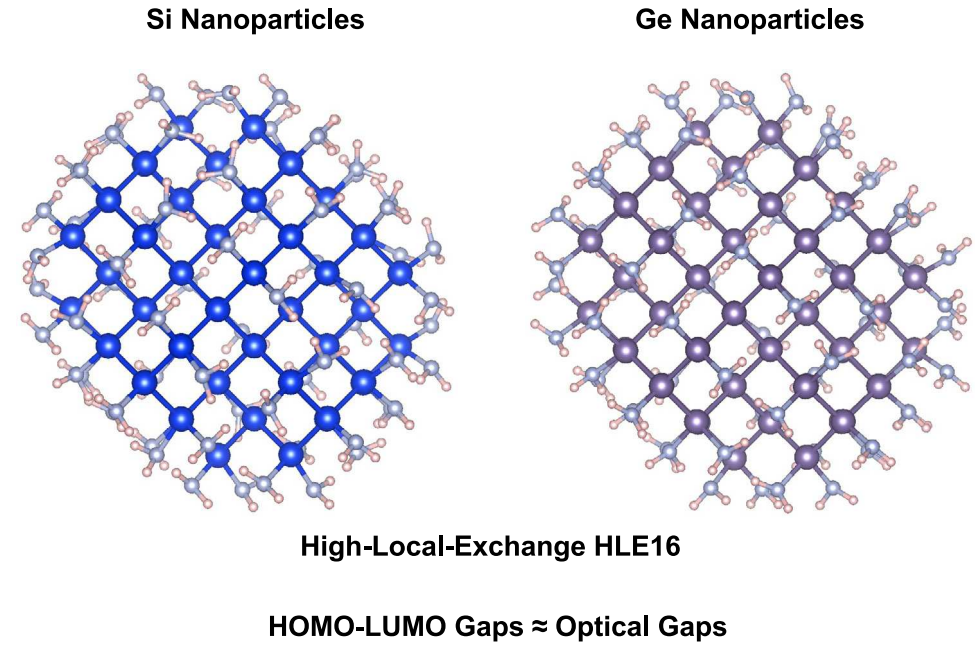

HIGHLIGHTS

- Reproduce optical gaps using ground-state high-local-exchange functional.
- Generate optical gaps w/o computational challenges of hybrid functionals and TDDFT.
- Control energy gaps via the interplay of quantum confinement and surface effects.
- Enhance the description of nanoparticles using effective core potentials.

ARTICLE INFO

Keywords:
Density functional theory
Nanoparticle

ABSTRACT

We investigated the HOMO-LUMO gaps and the optical gaps of Si and Ge nanoparticles (NPs) with various terminations and sizes using different functionals (HLE16, B3LYP, HSE-HJS) and basis sets (CRENBL, def2-SVP,

* Corresponding author.
E-mail address: laoku@vcu.edu (K.U. Lao).

https://doi.org/10.1016/j.cplett.2024.141460
Received 14 May 2024; Received in revised form 26 June 2024; Accepted 4 July 2024
Available online 8 July 2024

Effective core potential
Optical gap
HOMO- LUMO gap

def2-TZVP). The high-local-exchange functional HLE16, without Hartree–Fock exchange, effectively reproduces optical gaps using HOMO−LUMO gaps, offering a cost-effective alternative to hybrid functionals and TDDFT in nanoscale systems. Size (quantum confinement effects) and termination ligands (surface effects) significantly impact energy gaps: nonpolar CH_3 had minimal effects, while polar ligands reduced gaps notably. Finally, ECP basis sets like CRENBL are better suited for NP electronic structures than all-electron basis sets.

1. Introduction

The investigation and manipulation of the electronic structure of nanoparticles (NPs) with Group-14 elements like silicon (Si) and germanium (Ge), particularly focusing on the band gap [1], have gained increasingly important in advancing low-cost optoelectronics and photovoltaics [2,3]. The optoelectronic characteristics of these NPs can be tailored by adjusting their sizes (quantum confinement) or utilizing different surface ligands for passivation (surface chemistry) [4]. Computational modeling, especially through density functional theory (DFT), has been extensively employed due to challenges in precisely determining nanocluster sizes and investigating substitution effects from experiments, especially for very small nanoclusters. This computational approach enables a detailed examination of the electronic structure and optical properties, including the DFT-calculated orbital energy gap between the highest occupied molecular orbital (HOMO) and lowest unoccupied molecular orbital (LUMO), as well as the optical gap determined using linear-response time-dependent DFT (TDDFT). While accurately and efficiently determining these gaps is crucial for designing and discovering new materials with desired properties, it has remained a persistent challenge in quantum chemistry.

Passivating the surface mainly with atomic hydrogen is common due to computational cost considerations [5–8]. Other ligands used to passivate the surface of Si NPs have also been investigated, including halogen [9–14], double-bonded oxygen [15–17], hydroxyl groups (OH) [9,10,12,16–20], amino groups (NH_2) [9–12,18–20], and alkyl groups [9,10,12,21]. These investigations mainly used the hybrid B3LYP functional because its inclusion of nonlocal Hartree−Fock exchange can address the well-known tendency of local functionals to underestimate the band gap or orbital gap [22–27]. To the best of our knowledge, only one study has aimed to theoretically investigate the effects of surface passivation on three-dimensional Ge NPs using the B3LYP method [28]. The limited study of Ge NPs may be attributed to the significantly higher computational cost associated with Ge NPs compared to Si NPs of the same size. However, these studies mostly limit the size of NPs to less than 2 nm due to the high computational cost associated with hybrid functionals. Hybrid functionals increase the computational cost by at least an order of magnitude compared to local functionals, depending on the specific functionals used, the systems being studied, and the computer programs employed. The computational challenge of obtaining optical gaps using TDDFT is even more significant due to the computational cost per state and the large memory requirements of the iterative eigensolver [29]. This can render TDDFT calculations intractable for large systems, especially when using high-quality basis sets, or necessitate substantial high-performance computing resources. Since the HOMO−LUMO gap can approximate the optical gap [30,31], it is beneficial if the DFT-computed HOMO−LUMO gap accurately reflects the optical gap in practical terms.

To overcome the computational challenges for obtaining optical gaps using time-consuming hybrid functionals and TDDFT, this work demonstrates that a low-cost, high-local-exchange density functional without Hartree−Fock exchange can accurately reproduce the TDDFT optical gap for NPs by utilizing the ground state HOMO−LUMO gap. The high-local-exchange strategy provides an efficient method for determining the optical gap across systems of various sizes and with different ligands, ensuring consistent accuracy. Specifically, the high local exchange 2016 (HLE16) functional [23], which has been demonstrated to yield good results for band gaps and perform similarly to the well-established hybrid HSE06 functional [27], will be used in this work. HLE16 is a generalized gradient approximation (GGA) functional specifically calibrated to adjust the exchange and correlation components of HCTH/407 [32] by factors of 1.25 and 0.50, respectively. These empirical adjustments were carefully selected to ensure that HLE16 provides accurate predictions for the band gaps of solids and excitation energies of molecules [23].

2. Computational details

In this study, we use core structures of Si spherical-shaped NPs with diameters of 1.35 nm and 2.38 nm, comprising 68 and 286 Si atoms, respectively. Similarly, core structures of Ge spherical-shaped NPs with diameters of 1.41 nm and 2.48 nm, containing 68 and 286 Ge atoms, respectively, are also examined. These core structures were constructed using the cluster module of the Atomic Simulation Environment (ASE) library in Python [33], with lattice constants of 5.431 Å for Si NPs and 5.658 Å for Ge NPs. The diameters were defined as the maximum distance between any two heavy atoms within the NPs. Their fully H-passivated structures, $Si_{68}H_{66}$, $Si_{286}H_{158}$, $Ge_{68}H_{66}$, and $Ge_{286}H_{158}$, were fully optimized using the SPW92/def2-SVP level of theory [34–36], which has been demonstrated to reliably reproduce experimental lattice constants [37]. Additionally, other fully terminated Si and Ge cores were studied using different functional groups to account for their embedding in various dielectric matrices, including F, NH_2, OH, and CH_3, corresponding to metal fluoride, Si_3N_4, SiO_2, and SiC, respectively [9]. The core structures were held fixed at their corresponding H-passivated configurations, while only the structures of the functional groups were optimized using the GFN0-xTB method [38] with the xtb program package [39]. The HOMO−LUMO gaps of 1.4 nm Si and Ge NPs passivated by H, F, NH_2, OH, and CH_3 were calculated using the HLE16 functional [23], the popular B3LYP functional, and the well-established HSE-HJS functional (screened-exchange HSE06 using the updated HJS PBE exchange hole model) [40,41]. The hybrid B3LYP functional is used in this work due to its popularity in investigating energy gaps for nanoparticles, while the hybrid HSE-HJS functional is chosen for its well-known good performance in energy gap calculations. TDDFT calculations, both with and without the Tamm−Dancoff approximation (TDA) [42], were employed to determine the optical gap. In TDDFT, the optical gap is defined as the energy of the lowest allowed electronic transition, which corresponds to transitions with nonzero oscillator strength. We observed that TDDFT calculations with and without employing TDA yield the same excitation energies in both Si and Ge NPs, therefore only TDDFT/TDA will be discussed below. The CRENBL basis set with corresponding effective core potentials (ECPs) [43,44] on C, N, O, F, Si, and Ge was used for all these calculations. Additionally, the all-electron Karlsruhe basis sets, double-ζ def2-SVP and triplet-ζ def2-TZVP [36], were also employed for these calculations due to their good performance with DFT and their availability for nearly all elements in the periodic table. It is worth noting that previous computational studies on Si and Ge NPs utilized small double-ζ basis sets to determine ligand effects on the HOMO−LUMO and optical gaps. This work represents the first investigation of these gap values using both the Gaussian basis set with ECPs (CRENBL) and the triple-ζ basis set (def2-TZVP). Both HOMO−LUMO and optical gaps of 2.4 nm Si and Ge NPs with H terminations were explored using the HLE16/CRENBL level of theory. Since nearly identical values were found for both HOMO−LUMO and optical gaps in all the aforementioned calculations shown in this work, the effects of F, OH, NH_2,

Table 1
The HOMO–LUMO gaps (ΔE_{HL}) and the optical gaps (ΔE_{OptG}) in eV were calculated for 1.35 nm of Si NPs with surface terminations of H, F, NH_2, OH, and CH_3 using DFT and TDDFT/TDA methods, respectively. The calculations employed the HLE16, B3LYP, and HSE-HJS functionals with the CRENBL basis set. The response shift (RS) is defined as the difference between ΔE_{OptG} and ΔE_{HL}.

Ligand	HLE16			B3LYP			HSE-HJS		
	ΔE_{HL}	ΔE_{OptG}	RS	ΔE_{HL}	ΔE_{OptG}	RS	ΔE_{HL}	ΔE_{OptG}	RS
H	3.81	3.82	0.01	4.41	3.88	−0.53	3.81	3.70	−0.11
F	2.83	2.85	0.02	3.54	3.06	−0.48	2.97	2.90	−0.07
NH_2	2.23	2.22	−0.01	3.05	2.63	−0.42	2.50	2.47	−0.03
OH	2.07	2.09	0.02	2.64	2.27	−0.37	2.12	2.08	−0.04
CH_3	3.21	3.23	0.02	4.00	3.51	−0.49	3.43	3.33	−0.10

and CH_3 ligands on 2.4 nm Si and Ge NPs were solely investigated based on the HOMO–LUMO gaps at the HLE16/CRENBL level. The response shift (RS) [30], defined as the difference between the optical gap and the HOMO–LUMO gap, was employed to quantify the disparity between them. All Si and Ge NPs considered here exhibit a closed-shell electronic structure in the ground state. The most time-consuming calculation in this study involves the 2.48 nm Ge NP terminated by CH_3, which consists of 918 atoms and requires 13,102 basis functions using the CRENBL basis set. All DFT calculations for HOMO–LUMO gaps and TDDFT calculations, both with and without TDA, for optical gaps were carried out using a locally modified version of Q-Chem [45].

3. Results and discussion

3.1. Silicon nanoparticles

The HOMO–LUMO gaps (ΔE_{HL}) and the optical gaps (ΔE_{OptG}) for 1.35 nm of Si NPs with various surface terminations and different computational methods are presented in Table 1. ΔE_{HL} and ΔE_{OptG} exhibit very good agreement, with RS ranging from −0.01 to 0.04 eV using HLE16. This indicates that ΔE_{HL} serves as a reliable approximation for ΔE_{OptG}, making it a viable substitute in cases where TDDFT calculations are not feasible. It has been demonstrated that there exists a strong correlation between RS and the proportion of Hartree–Fock exchange integrated into the hybrid density functional [30]. Hybrid functionals incorporating around 10% of Hartree–Fock exchange may produce an average RS of zero, thereby aligning ΔE_{HL} more closely with molecular excitation energies [30]. Our work here indicates that ΔE_{HL} can effectively approximate ΔE_{OptG} when using the high-local-exchange HLE16 functional, even in the absence of the computationally demanding Hartree–Fock exchange. For HSE-HJS, which is commonly used in energy gap calculations, the RS values range slightly larger from −0.11 to −0.03 eV, making ΔE_{HL} still a good approximation for ΔE_{OptG}. The mean absolute deviation (MAD) between ΔE_{HL} from HLE16 and ΔE_{OptG} from the more time-consuming hybrid functional HSE-HJS is just 0.11 eV, highlighting their close agreement. B3LYP exhibits a larger RS range from −0.49 to −0.33 eV, indicating that ΔE_{HL} cannot effectively represent ΔE_{OptG}. The largest deviation, with an RS of −0.49 eV, occurs with the hydrogen termination. This value aligns with previous observations that ΔE_{OptG} of large H-passivated Si NPs can be estimated by adding a constant correction of −0.5 eV to ΔE_{HL} at the B3LYP level [5,15].

The ligand significantly impacts the electronic structure of Si NPs, leading to a significant reduction in both ΔE_{HL} and ΔE_{OptG}. The gaps decrease in the following order of ligands: H > CH_3 > F > NH_2 > OH for all three functionals, indicating an increase in optical activity. This observation aligns with previous findings for Si NPs of similar size [9]. The gaps are influenced weakly by replacing H by a nonpolar ligand CH_3, resulting in reductions of ΔE_{HL} by 0.6, 0.4, and 0.4 eV using HLE16, B3LYP, and HSE-HJS, respectively. This observation aligns with previous studies indicating that changing the termination from H to CH_3 has little impact on the ΔE_{HL} of Si NPs [9,21,46]. Polar ligands

Table 2
The HOMO–LUMO gaps in eV were calculated for different sizes of Si and Ge NPs with surface terminations of H, F, NH_2, OH, and CH_3 using HLE16/CRENBL. The Δ_{size} value in eV represents the reduction in ΔE_{HL} by increasing the NPs by approximately 1 nm.

Ligand	Si			Ge		
	1.35 nm	2.38 nm	Δ_{size}	1.41 nm	2.48 nm	Δ_{size}
H	3.81	2.69	−1.12	3.27	2.18	−1.09
F	2.83	2.45	−0.38	2.15	1.58	−0.57
NH_2	2.23	2.07	−0.16	1.55	1.09	−0.46
OH	2.07	1.61	−0.46	1.80	1.50	−0.30
CH_3	3.21	2.48	−0.73	2.69	1.90	−0.79

Table 3
The HOMO–LUMO gaps (ΔE_{HL}) and the optical gaps (ΔE_{OptG}) in eV were calculated for 1.35 nm of Si NPs with surface terminations of H, F, NH_2, OH, and CH_3 using DFT and TDDFT/TDA methods, respectively. The calculations employed the HLE16 functional with all-electron def2-SVP and def2-TZVP basis sets. The response shift (RS) is defined as the difference between ΔE_{OptG} and ΔE_{HL}.

Ligand	def2-SVP			def2-TZVP		
	ΔE_{HL}	ΔE_{OptG}	RS	ΔE_{HL}	ΔE_{OptG}	RS
H	3.48	3.50	0.02	3.46	3.46	0.00
F	2.69	2.70	0.01	2.67	2.69	0.02
NH_2	2.39	2.40	0.01	2.42	2.41	−0.01
OH	2.15	2.16	0.01	2.12	2.13	0.01
CH_3	2.99	3.03	0.04	2.97	3.00	0.03

can significantly impact the electronic structure of NPs, resulting in large reductions in the gaps. For 1.35 nm Si NPs, replacing H by F, NH_2, and OH ligands can reduce the gaps by 1.0, 1.6, and 1.7 eV, respectively. Additionally, experimental findings have shown that the photoluminescence (PL) of H-passivated Si NPs undergoes a red shift after exposure to oxygen [47], and the PL of Si NPs embedded in Si_3N_4 undergoes a blue shift compared to Si NPs of the same size embedded in SiO_2 [48]. These observations align with our research, where we observe a reduction in gaps via redshift from H to OH ligands, and an increase in gaps via blue shift from OH to NH_2 ligands.

For the Si NP passivated with H and having a diameter of 2.38 nm, ΔE_{HL} again exhibits very good agreement with ΔE_{OptG}, with an RS value of 0.01 eV. Therefore, we exclusively use ΔE_{HL} at the HLE16/CERNBL level to discuss the gap change of Si NPs when increasing the size from 1.35 to 2.38 nm, as shown in Table 2. For larger sizes of silicon NPs, the gaps decrease in the same order of ligands as the smaller NPs. However, the influence of the interface termination decreases with increasing NP size. The ΔE_{HL} value of the Si NP, passivated with H, decreases significantly by 1.12 eV when its size increases by approximately 1 nm. The nonpolar ligand CH_3 reduces the size effect to 0.73 eV. The three polar ligands, F, NH_2, and OH, show relatively small size effects by reducing the gaps by 0.38, 0.16, and 0.46 eV, respectively. The ΔE_{HL} values of NPs with polar ligands do not significantly change with an increase in the size of the Si core. This indicates that polar ligands play a crucial role in governing the electronic structure of Si NPs and mitigating the impact of quantum confinement as compared to Si NPs with nonpolar ligands. In other words, the interface termination can counteract the effects of quantum confinement. Of all tested ligands for Si NPs, the OH ligand exhibits the most significant reduction in the gap at the same core size, while NH_2 demonstrates the most effective reduction in quantum confinement effects through size variation.

The Si NPs with diameters of 1.35 nm and all five passivations were calculated using the all-electron def2-SVP and def2-TZVP basis sets with HLE16 as shown in Table 3. It is clear that both all-electron basis sets exhibit very small values of RS for all ligands, indicating that the close-to-zero RS is not due to ECPs. Additionally, both basis sets exhibit very similar ΔE_{HL} and ΔE_{OptG} values, with a maximum deviation of only 0.04 eV observed for the H-passivated NP in ΔE_{OptG}. Thus, the def2-SVP basis set can be considered as a converged all-electron basis

Table 4
The HOMO–LUMO gaps (ΔE_{HL}) and the optical gaps (ΔE_{OptG}) in eV were calculated for 1.41 nm of Ge NPs with surface terminations of H, F, NH_2, OH, and CH_3 using DFT and TDDFT/TDA methods, respectively. The calculations employed the HLE16, B3LYP, and HSE-HJS functionals with the CRENBL basis set. The response shift (RS) is defined as the difference between ΔE_{OptG} and ΔE_{HL}.

Ligand	HLE16			B3LYP			HSE-HJS		
	ΔE_{HL}	ΔE_{OptG}	RS	ΔE_{HL}	ΔE_{OptG}	RS	ΔE_{HL}	ΔE_{OptG}	RS
H	3.27	3.31	0.04	3.92	3.43	−0.49	3.43	3.33	−0.10
F	2.15	2.15	0.00	2.91	2.45	−0.46	2.48	2.41	−0.07
NH_2	1.55	1.55	0.00	2.53	2.19	−0.34	2.10	2.06	−0.04
OH	1.80	1.79	−0.01	2.50	2.17	−0.33	2.07	2.05	−0.02
CH_3	2.69	2.70	0.01	3.54	3.07	−0.47	3.16	3.07	−0.09

Table 5
The HOMO–LUMO gaps (ΔE_{HL}) and the optical gaps (ΔE_{OptG}) in eV were calculated for 1.41 nm of Ge NPs with surface terminations of H, F, NH_2, OH, and CH_3 using DFT and TDDFT/TDA methods, respectively. The calculations employed the HLE16 functional with all-electron def2-SVP and def2-TZVP basis sets. The response shift (RS) is defined as the difference between ΔE_{OptG} and ΔE_{HL}.

Ligand	def2-SVP			def2-TZVP		
	ΔE_{HL}	ΔE_{OptG}	RS	ΔE_{HL}	ΔE_{OptG}	RS
H	3.51	3.53	0.02	3.48	3.46	−0.02
F	2.50	2.51	0.01	2.53	2.54	0.01
NH_2	2.01	2.03	0.02	2.10	2.09	−0.01
OH	2.23	2.24	0.01	2.31	2.31	0.00
CH_3	2.99	3.00	0.01	2.97	2.99	0.02

set for conducting ΔE_{HL} and ΔE_{OptG} calculations in Si NPs. Compared to CRENBL, ΔE_{HL} exhibits deviations of up to 0.33 eV for the H-passivated NP when using def2-SVP. Specifically, the H, F, and CH_3 terminations display smaller ΔE_{HL} values with def2-SVP compared to CRENBL. Conversely, the NH_2 and OH terminations demonstrate larger ΔE_{HL} values with def2-SVP compared to CRENBL. However, we will demonstrate below that CRENBL is a more suitable basis set for NP calculations when comparing ΔE_{HL} values between Si and Ge NPs. This preference may be attributed to the proper treatment of relativistic effects in the CRENBL ECP.

3.2. Germanium nanoparticles

The ΔE_{HL} and ΔE_{OptG} values for Ge NPs with diameters of 1.41 nm, terminated by the same five ligands, are detailed in Table 4 using HLE16, B3LYP, and HSE-HJS with CRENBL. The results for Ge NPs using HLE16 mirror those of Si NPs, with RS values near zero (from −0.01 to 0.04 eV), signifying the reliability of using ΔE_{HL} to approximate ΔE_{OptG} without necessitating Hartree–Fock exchange. Similarly, RS values for HSE-HJS are slightly larger, ranging from −0.10 to −0.02 eV, while for B3LYP, they are significantly larger, ranging from −0.49 to −0.33 eV. The MAD between ΔE_{HL} calculated using HLE16 and ΔE_{OptG} obtained from the more time-consuming hybrid functional HSE-HJS is 0.29 eV, which is higher than that observed for Si NPs. The decrease in gaps follows the same order observed for Si NPs: H > CH_3 > F > NH_2 > OH using B3LYP and HSE-HJS. Notably, the difference in energy gap between NH_2 and OH is only 0.03 eV. However, when using HLE16, the gap order for NH_2 and OH reverses, with OH > NH_2 by 0.25 eV for ΔE_{HL} or 0.24 eV for ΔE_{OptG}. Similar to Si NPs, the gaps are weakly influenced by replacing H with a nonpolar ligand CH_3, resulting in reductions of ΔE_{HL} by 0.6, 0.4, and 0.3 eV using HLE16, B3LYP, and HSE-HJS, respectively. The three polar ligands show gap reductions in the range of 1.1–1.7 eV, 1.0–1.4 eV, and 1.0–1.4 eV when using HLE16, B3LYP, and HSE-HJS, respectively.

For the Ge NP passivated with H and having a diameter of 2.48 nm, ΔE_{HL} once again shows very good agreement with ΔE_{OptG}, with an RS value of 0.01 eV at the HLE16/CERNBL level. Regarding the 2.48 nm Ge NPs, the gaps decrease in the same order of ligands as the smaller NPs. As with Si NPs, the impact of the interface termination diminishes as the size of Ge NPs increases. The ΔE_{HL} of the H-passivated Ge NP reduces notably by 1.09 eV as its size increases by approximately 1 nm, mirroring a similar reduction of 1.12 eV seen in the corresponding Si NP. The nonpolar ligand CH_3 diminishes the size effect to 0.79 eV, a value similar to the 0.73 eV observed in the corresponding Si NP. The polar ligands F, NH_2, and OH demonstrate modest impacts on size, reducing the gaps by 0.57, 0.46, and 0.30 eV, respectively. This further illustrates how polar ligands can mitigate the impact of quantum confinement, leading to smaller changes in the energy gap related to size variations. Of all the ligands tested for Ge NPs, NH_2 shows the most significant reduction in the gap for the same size of NP, while OH is most effective in mitigating quantum confinement effects by adjusting its size. This observation differs from the trends observed in Si NPs. Thus, NH_2 and OH ligands can uniquely influence the properties of Si and Ge NPs, leading to modifications in energy gaps and quantum confinement effects. These distinct effects offer an efficient strategy to customize the desired optical properties across different Si and Ge NP sizes.

We utilized the all-electron def2-SVP and def2-TZVP basis sets with HLE16 to calculate RS values and assess the influence of ligands on the energy gaps of Ge NPs as shown in Table 5. The obtained RS values are consistently close to zero, indicating the suitability of using ΔE_{HL} to represent ΔE_{OptG} in Ge NPs as well. Both basis sets demonstrate very similar ΔE_{HL} and ΔE_{OptG} values, with the NH_2-passivated NP showing a maximum deviation of only 0.09 eV in ΔE_{HL}. This deviation, although slightly larger than the 0.04 eV maximum observed for Si NPs, remains quite small. The def2-SVP basis set continues to be a converged all-electron basis set for conducting calculations involving ΔE_{HL} and ΔE_{OptG} in Ge NPs, eliminating the need for triplet-ζ basis sets. Compared to CRENBL, there are deviations of up to 0.46 eV in ΔE_{HL} for the NH_2-passivated NP when using def2-SVP. For NPs with all five different terminations, the energy gaps (ΔE_{HL} or ΔE_{OptG}) are larger for 1.35 nm Si NPs compared to 1.41 nm Ge NPs when using CRENBL. This trend aligns with the bulk energy gaps of Si (1.17 eV) and Ge (0.74 eV) at 0 K [49]. However, this trend is not consistent for H-, OH-, and CH_3-passivated NPs when using both all-electron basis sets. This discrepancy may arise from the inclusion of relativistic effects in the CRENBL ECP, which are not accounted for in all-electron def2-SVP and def2-TZVP basis sets, especially for Ge NPs. Therefore, it is recommended to utilize ECP basis sets when calculating Si and Ge NPs, as they not only offer faster computations but also capture the relevant physics accurately.

4. Conclusions

We investigated HOMO–LUMO and optical gaps of Si and Ge NPs with five different terminations (H, F, NH_2, OH, CH_3) and two sizes (1.4 and 2.4 nm) using various DFT functionals (HLE16, B3LYP, HSE-HJS) and basis sets (CRENBL, def2-SVP, def2-TZVP). While a previous study suggested including approximately 10% of Hartree–Fock exchange to reproduce the optical gaps using only HOMO–LUMO gaps [30], our results show that the high-local-exchange functional HLE16 achieves the same outcome for NPs without costly Hartree–Fock exchange. This provides a practical and cost-effective strategy in generating optical gaps using ground state HLE16 calculations at relatively low cost without computational challenges from hybrid functionals and TDDFT, therefore recommended for nanostructures where the high cost of hybrid functionals or TDDFT can make them impractical for such applications. This efficient approach also facilitates the generation of large datasets for training machine learning models to predict optical gaps without relying on *ab initio* calculations [50], especially given the limited availability of reliable experimental data for NPs. It should be noted that TDDFT calculations are still necessary if the optical spectrum, not just the gap, is required.

Moreover, our study highlights the impact of size and termination ligands on energy gaps in Si and Ge NPs. Nonpolar ligands like CH_3 have minimal effects on gaps compared to H, while polar ligands (F, NH_2, and OH) can significantly reduce gaps. The interface between the NP and ligand plays a crucial role in determining electronic structure, competing with quantum confinement effects. For Si NPs, the OH ligand exhibits the largest reduction in energy gaps, while NH_2 mitigates quantum confinement effects. In contrast, NH_2 is most effective in reducing gaps for Ge NPs, with OH being effective in mitigating quantum confinement effects. Overall, the interplay between quantum confinement and interface termination influences the electronic and optical gap engineering of Si and Ge NPs. Lastly, ECP basis sets like CRENBL are better suited for describing NP electronic structures compared to all-electron basis sets, as indicated by our results aligning with bulk trends.

CRediT authorship contribution statement

Corentin Villot: Writing – review & editing, Writing – original draft, Visualization, Software, Data curation, Conceptualization. **Ka Un Lao:** Writing – review & editing, Writing – original draft, Visualization, Validation, Supervision, Software, Resources, Project administration, Methodology, Investigation, Funding acquisition, Formal analysis, Data curation, Conceptualization.

Declaration of competing interest

The authors declare that they have no known competing financial interests or personal relationships that could have appeared to influence the work reported in this paper.

Data availability

Data will be made available on request.

Acknowledgments

This work was supported by the National Science Foundation, United States through grant DMR-2211606. C.V. acknowledges the generous support of the VCU Graduate School Dissertation Assistantship. High Performance Computing resources provided by the High Performance Research Computing (HPRC) Core Facility at Virginia Commonwealth University (https://chipc.vcu.edu) were used for conducting the research reported in this work.

References

[1] J.P. Perdew, W. Yang, K. Burke, Z. Yang, E.K.U. Gross, M. Scheffler, G.E. Scuseria, T.M. Henderson, I.Y. Zhang, A. Ruzsinszky, H. Peng, J. Sun, E. Trushin, A. Görling, Understanding band gaps of solids in generalized Kohn–Sham theory, Proc. Natl. Acad. Sci. USA 114 (2017) 2801–2806, http://dx.doi.org/10.1073/pnas.1621352114.

[2] C. Zhang, Z. Li, X. Deng, B. Yan, Z. Wang, X. Chen, Z. Sun, S. Huang, Enhancing photovoltaic performance of perovskite solar cells utilizing germanium nanoparticles, Sol. Energy 188 (2019) 839–848, http://dx.doi.org/10.1016/j.solener.2019.06.069.

[3] D. Beri, Silicon quantum dots: surface matter, what next? Mater. Adv. 4 (2023) 3380–3398, http://dx.doi.org/10.1039/D2MA00984F.

[4] P. Makkar, N.N. Ghosh, A review on the use of DFT for the prediction of the properties of nanomaterials, RSC Adv. 11 (2021) 27897–27924, http://dx.doi.org/10.1039/D1RA04876G.

[5] C.S. Garoufalis, A.D. Zdetsis, S. Grimme, High level ab initio calculations of the optical gap of small silicon quantum dots, Phys. Rev. Lett. 87 (2001) 276402, http://dx.doi.org/10.1103/PhysRevLett.87.276402.

[6] X. Zheng, A.J. Cohen, P. Mori-Sánchez, X. Hu, W. Yang, Improving band gap prediction in density functional theory from molecules to solids, Phys. Rev. Lett. 107 (2011) 026403, http://dx.doi.org/10.1103/PhysRevLett.107.026403.

[7] N.C. Forero-Martinez, H.-L. Thi Le, N. Ning, H. Vach, H.-C. Weissker, Temperature dependence of the radiative lifetimes in Ge and Si nanocrystals, Nanoscale 7 (2015) 4942–4948, http://dx.doi.org/10.1039/C4NR04905E.

[8] S. Niaz, A.D. Zdetsis, Comprehensive ab initio study of electronic, optical, and cohesive properties of silicon quantum dots of various morphologies and sizes up to infinity, J. Phys. Chem. C 120 (2016) 11288–11298, http://dx.doi.org/10.1021/acs.jpcc.6b02955.

[9] D. König, J. Rudd, M.A. Green, G. Conibeer, Role of the interface for the electronic structure of Si quantum dots, Phys. Rev. B 78 (2008) 035339, http://dx.doi.org/10.1103/PhysRevB.78.035339.

[10] D. König, J. Rudd, M. Green, G. Conibeer, Impact of interface on the effective band gap of Si quantum dots, Sol. Energy Mater. Sol. Cells 93 (2009) 753–758, http://dx.doi.org/10.1016/j.solmat.2008.09.026.

[11] A. Martínez, J.C. Alonso, L.E. Sansores, R. Salcedo, Electronic structure of silicon nanocrystals passivated with nitrogen and chlorine, J. Phys. Chem. C 114 (2010) 12427–12431, http://dx.doi.org/10.1021/jp102017d.

[12] W.-H. Chen, C.-H. Chang, Y.-S. Chang, J.-H. Pan, H.-W. Wang, Y.-M. Chou, B.-C. Wang, Effect of passivants in energy gap of $Si_{47}X_{24}Y_{36}$ nano-clusters: A theoretical investigation, Physica E 43 (2011) 948–953, http://dx.doi.org/10.1016/j.physe.2010.11.023.

[13] R. Wang, X. Pi, D. Yang, Surface modification of chlorine-passivated silicon nanocrystals, Phys. Chem. Chem. Phys. 15 (2013) 1815–1820, http://dx.doi.org/10.1039/C2CP43763E.

[14] N.V. Derbenyova, A.A. Konakov, A.E. Shvetsov, V.A. Burdov, Electronic structure and absorption spectra of silicon nanocrystals with a halogen (Br, Cl) coating, JETP Lett. 106 (2017) 247–251, http://dx.doi.org/10.1134/S0021364017160068.

[15] C.S. Garoufalis, A.D. Zdetsis, High accuracy calculations of the optical gap and absorption spectrum of oxygen contaminated Si nanocrystals, Phys. Chem. Chem. Phys. 8 (2006) 808–813, http://dx.doi.org/10.1039/B513184G.

[16] Z. Zhou, L. Brus, R. Friesner, Electronic structure and luminescence of 1.1- and 1.4-nm silicon nanocrystals: Oxide shell versus hydrogen passivation, Nano Lett. 3 (2003) 163–167, http://dx.doi.org/10.1021/nl025890q.

[17] D. König, J. Rudd, G. Conibeer, M. Green, Impact of bridge- and double-bonded oxygen on OH-terminated Si quantum dots: A density-functional–Hartree–Fock study, Mater. Sci. Eng. B 159–160 (2009) 117–121, http://dx.doi.org/10.1016/j.mseb.2008.11.022.

[18] D. König, D. Hiller, S. Gutsch, M. Zacharias, Energy offset between silicon quantum structures: Interface impact of embedding dielectrics as doping alternative, Adv. Mater. Interfaces 1 (2014) 1400359, http://dx.doi.org/10.1002/admi.201400359.

[19] D. König, Y. Yao, S. Smith, Bridge- and double-bonded O and NH on fully OH- and NH_2-terminated silicon nanocrystals: Ground and excited state properties, Phys. Status Solidi b 256 (2019) 1800336, http://dx.doi.org/10.1002/pssb.201800336.

[20] D. König, D. Hiller, S.C. Smith, Absorption and photoluminescence of silicon nanocrystals investigated by excited state DFT: Role of embedding dielectric and defects, Phys. Status Solidi b 259 (2022) 2100549, http://dx.doi.org/10.1002/pssb.202100549.

[21] F.A. Reboredo, G. Galli, Theory of alkyl-terminated silicon quantum dots, J. Phys. Chem. B 109 (2005) 1072–1078, http://dx.doi.org/10.1021/jp0462254.

[22] H. Xiao, J. Tahir-Kheli, W.A.I. Goddard, Accurate band gaps for semiconductors from density functional theory, J. Phys. Chem. Lett. 2 (2011) 212–217, http://dx.doi.org/10.1021/jz101565j.

[23] P. Verma, D.G. Truhlar, HLE16: A local Kohn–Sham gradient approximation with good performance for semiconductor band gaps and molecular excitation energies, J. Phys. Chem. Lett. 8 (2017) 380–387, http://dx.doi.org/10.1021/acs.jpclett.6b02757.

[24] P. Verma, D.G. Truhlar, HLE17: An improved local exchange–correlation functional for computing semiconductor band gaps and molecular excitation energies, J. Phys. Chem. C 121 (2017) 7144–7154, http://dx.doi.org/10.1021/acs.jpcc.7b01066.

[25] I. Choudhuri, D.G. Truhlar, HLE17: An efficient way to predict band gaps of complex materials, J. Phys. Chem. C 123 (2019) 17416–17424, http://dx.doi.org/10.1021/acs.jpcc.9b04683.

[26] P. Borlido, T. Aull, A.W. Huran, F. Tran, M.A.L. Marques, S. Botti, Large-scale benchmark of exchange–correlation functionals for the determination of electronic band gaps of solids, J. Chem. Theory Comput. 15 (2019) 5069–5079, http://dx.doi.org/10.1021/acs.jctc.9b00322.

[27] P. Borlido, J. Schmidt, A.W. Huran, F. Tran, M.A.L. Marques, S. Botti, Exchange–correlation functionals for band gaps of solids: benchmark, reparametrization and machine learning, NPJ Comput. Mater. 6 (2020) 96, http://dx.doi.org/10.1038/s41524-020-00360-0.

[28] Shanawer Niaz, Oğuz Gülseren, Safdar Hussain, M. Anwar-ul Haq, Manzoor Ahmad Badar, Muhammad Aslam Khan, Theoretical study of germanium nanoclusters: significance of surface passivation, Eur. Phys. J. Plus 137 (2022) 316, http://dx.doi.org/10.1140/epjp/s13360-022-02502-3.

[29] M.W.D. Hanson-Heine, M.W. George, N.A. Besley, Assessment of time-dependent density functional theory with the restricted excitation space approximation for excited state calculations of large systems, Mol. Phys. 116 (2018) 1452–1459, http://dx.doi.org/10.1080/00268976.2018.1430388.

[30] Y. Shu, D.G. Truhlar, Relationships between orbital energies, optical and fundamental gaps, and exciton shifts in approximate density functional theory and quasiparticle theory, J. Chem. Theory Comput. 16 (2020) 4337–4350, http://dx.doi.org/10.1021/acs.jctc.0c00320.

[31] B.G. Janesko, Replacing hybrid density functional theory: motivation and recent advances, Chem. Soc. Rev. 50 (2021) 8470–8495, http://dx.doi.org/10.1039/D0CS01074J.

[32] A.D. Boese, N.C. Handy, A new parametrization of exchange–correlation generalized gradient approximation functionals, J. Chem. Phys. 114 (2001) 5497–5503, http://dx.doi.org/10.1063/1.1347371.

[33] A.H. Larsen, J.J. Mortensen, J. Blomqvist, I.E. Castelli, R. Christensen, M. Dułak, J. Friis, M.N. Groves, B. Hammer, C. Hargus, E.D. Hermes, P.C. Jennings, P.B. Jensen, J. Kermode, J.R. Kitchin, E.L. Kolsbjerg, J. Kubal, K. Kaasbjerg, S. Lysgaard, J.B. Maronsson, T. Maxson, T. Olsen, L. Pastewka, A. Peterson, C. Rostgaard, J. Schiøtz, O. Schütt, M. Strange, K.S. Thygesen, T. Vegge, L. Vilhelmsen, M. Walter, Z. Zeng, K.W. Jacobsen, The atomic simulation environment—a python library for working with atoms, J. Phys.: Condens. Matter. 29 (2017) 273002, http://dx.doi.org/10.1088/1361-648X/aa680e.

[34] P.A.M. Dirac, Note on exchange phenomena in the Thomas atom, Math. Proc. Camb. Philos. Soc. 26 (1930) 376–385, http://dx.doi.org/10.1017/S0305004100016108.

[35] J.P. Perdew, Y. Wang, Accurate and simple analytic representation of the electron-gas correlation energy, Phys. Rev. B 45 (1992) 13244–13249, http://dx.doi.org/10.1103/PhysRevB.45.13244.

[36] F. Weigend, R. Ahlrichs, Balanced basis sets of split valence, triple zeta valence and quadruple zeta valence quality for H to Rn: Design and assessment of accuracy, Phys. Chem. Chem. Phys. 7 (2005) 3297–3305, http://dx.doi.org/10.1039/B508541A.

[37] D. Spera, D. Pate, G.C. Spence, C. Villot, C.J. Onukwughara, D. White, K.U. Lao, Ü. Özgür, I.U. Arachchige, Colloidal synthesis of homogeneous $Ge_{1-x-y}Si_ySn_x$ nanoalloys with composition-tunable visible to near-IR optical properties, Chem. Mater. 35 (2023) 9007–9018, http://dx.doi.org/10.1021/acs.chemmater.3c01644.

[38] P. Pracht, E. Caldeweyher, S. Ehlert, S. Grimme, A robust non-self-consistent tight-binding quantum chemistry method for large molecules, 2019, http://dx.doi.org/10.26434/chemrxiv.8326202.v1, ChemRxiv.

[39] C. Bannwarth, E. Caldeweyher, S. Ehlert, A. Hansen, P. Pracht, J. Seibert, S. Spicher, S. Grimme, Extended tight-binding quantum chemistry methods, Wiley Interdiscip. Rev. Comput. Mol. Sci. 11 (2021) e1493, http://dx.doi.org/10.1002/wcms.1493.

[40] A.V. Krukau, O.A. Vydrov, A.F. Izmaylov, G.E. Scuseria, Influence of the exchange screening parameter on the performance of screened hybrid functionals, J. Chem. Phys. 125 (2006) 224106, http://dx.doi.org/10.1063/1.2404663.

[41] T.M. Henderson, B.G. Janesko, G.E. Scuseria, Generalized gradient approximation model exchange holes for range-separated hybrids, J. Chem. Phys. 128 (2008) 194105, http://dx.doi.org/10.1063/1.2921797.

[42] S. Hirata, M. Head-Gordon, Time-dependent density functional theory within the Tamm–Dancoff approximation, Chem. Phys. Lett. 314 (1999) 291–299, http://dx.doi.org/10.1016/S0009-2614(99)01149-5.

[43] L. Fernandez Pacios, P.A. Christiansen, Ab initio relativistic effective potentials with spin–orbit operators. I. Li through Ar, J. Chem. Phys. 82 (1985) 2664–2671, http://dx.doi.org/10.1063/1.448263.

[44] M.M. Hurley, L.F. Pacios, P.A. Christiansen, R.B. Ross, W.C. Ermler, Ab initio relativistic effective potentials with spin–orbit operators. II. K through Kr, J. Chem. Phys. 84 (1986) 6840–6853, http://dx.doi.org/10.1063/1.450689.

[45] E. Epifanovsky, A.T.B. Gilbert, X. Feng, J. Lee, Y. Mao, N. Mardirossian, P. Pokhilko, A.F. White, M.P. Coons, A.L. Dempwolff, Z. Gan, D. Hait, P.R. Horn, L.D. Jacobson, I. Kaliman, J. Kussmann, A.W. Lange, K.U. Lao, D.S. Levine, J. Liu, S.C. McKenzie, A.F. Morrison, K.D. Nanda, F. Plasser, D.R. Rehn, M.L. Vidal, Z.-Q. You, Y. Zhu, B. Alam, B.J. Albrecht, A. Aldossary, E. Alguire, J.H. Andersen, V. Athavale, D. Barton, K. Begam, A. Behn, N. Bellonzi, Y.A. Bernard, E.J. Berquist, H.G.A. Burton, A. Carreras, K. Carter-Fenk, R. Chakraborty, A.D. Chien, K.D. Closser, V. Cofer-Shabica, S. Dasgupta, M. de Wergifosse, J. Deng, M. Diedenhofen, H. Do, S. Ehlert, P.-T. Fang, S. Fatehi, Q. Feng, T. Friedhoff, J. Gayvert, Q. Ge, G. Gidofalvi, M. Goldey, J. Gomes, C.E. González-Espinoza, S. Gulania, A.O. Gunina, M.W.D. Hanson-Heine, P.H.P. Harbach, A. Hauser, M.F. Herbst, M. Hernández Vera, M. Hodecker, Z.C. Holden, S. Houck, X. Huang, K. Hui, B.C. Huynh, M. Ivanov, Á. Jász, H. Ji, H. Jiang, B. Kaduk, S. Kähler, K. Khistyaev, J. Kim, G. Kis, P. Klunzinger, Z. Koczor-Benda, J.H. Koh, D. Kosenkov, L. Koulias, T. Kowalczyk, C.M. Krauter, K. Kue, A. Kunitsa, T. Kus, I. Ladjánszki, A. Landau, K.V. Lawler, D. Lefrancois, S. Lehtola, R.R. Li, Y.-P. Li, J. Liang, M. Liebenthal, H.-H. Lin, Y.-S. Lin, F. Liu, K.-Y. Liu, M. Loipersberger, A. Luenser, A. Manjanath, P. Manohar, E. Mansoor, S.F. Manzer, S.-P. Mao, A.V. Marenich, T. Markovich, S. Mason, S.A. Maurer, P.F. McLaughlin, M.F.S.J. Menger, J.-M. Mewes, S.A. Mewes, P. Morgante, J.W. Mullinax, K.J. Oosterbaan, G. Paran, A.C. Paul, S.K. Paul, F. Pavošević, Z. Pei, S. Prager, E.I. Proynov, Á. Rák, E. Ramos-Cordoba, B. Rana, A.E. Rask, A. Rettig, R.M. Richard, F. Rob, E. Rossomme, T. Scheele, M. Scheurer, M. Schneider, N. Sergueev, S.M. Sharada, W. Skomorowski, D.W. Small, C.J. Stein, Y.-C. Su, E.J. Sundstrom, Z. Tao, J. Thirman, G.J. Tornai, T. Tsuchimochi, N.M. Tubman, S.P. Veccham, O. Vydrov, J. Wenzel, J. Witte, A. Yamada, K. Yao, S. Yeganeh, S.R. Yost, A. Zech, I.Y. Zhang, X. Zhang, Y. Zhang, D. Zuev, A. Aspuru-Guzik, A.T. Bell, N.A. Besley, K.B. Bravaya, B.R. Brooks, D. Casanova, J.-D. Chai, S. Coriani, C.J. Cramer, G. Cserey, A.E. DePrince, R.A. DiStasio, A. Dreuw, B.D. Dunietz, T.R. Furlani, W.A. Goddard, S. Hammes-Schiffer, T. Head-Gordon, W.J. Hehre, C.-P. Hsu, T.-C. Jagau, Y. Jung, A. Klamt, J. Kong, D.S. Lambrecht, W. Liang, N.J. Mayhall, C.W. McCurdy, J.B. Neaton, C. Ochsenfeld, J.A. Parkhill, R. Peverati, V.A. Rassolov, Y. Shao, L.V. Slipchenko, T. Stauch, R.P. Steele, J.E. Subotnik, A.J.W. Thom, A. Tkatchenko, D.G. Truhlar, T. Van Voorhis, T.A. Wesolowski, K.B. Whaley, H.L. Woodcock, P.M. Zimmerman, S. Faraji, P.M.W. Gill, M. Head-Gordon, J.M. Herbert, A.I. Krylov, Software for the frontiers of quantum chemistry: An overview of developments in the Q-Chem 5 package, J. Chem. Phys. 155 (2021) 084801, http://dx.doi.org/10.1063/5.0055522.

[46] Q.S. Li, R.Q. Zhang, S.T. Lee, T.A. Niehaus, T. Frauenheim, Optimal surface functionalization of silicon quantum dots, J. Chem. Phys. 128 (2008) 244714, http://dx.doi.org/10.1063/1.2940735.

[47] M.V. Wolkin, J. Jorne, P.M. Fauchet, G. Allan, C. Delerue, Electronic states and luminescence in porous silicon quantum dots: The role of oxygen, Phys. Rev. Lett. 82 (1999) 197–200, http://dx.doi.org/10.1103/PhysRevLett.82.197.

[48] M.-S. Yang, K.-S. Cho, J.-H. Jhe, S.-Y. Seo, J.H. Shin, K.J. Kim, D.W. Moon, Effect of nitride passivation on the visible photoluminescence from Si-nanocrystals, Appl. Phys. Lett. 85 (2004) 3408–3410, http://dx.doi.org/10.1063/1.1787599.

[49] C. Kittel, Introduction to Solid State Physics, eighth ed., John Wiley & Sons Inc, 2004.

[50] R. Ramakrishnan, M. Hartmann, E. Tapavicza, O.A. von Lilienfeld, Electronic spectra from TDDFT and machine learning in chemical space, J. Chem. Phys. 143 (2015) 084111, http://dx.doi.org/10.1063/1.4928757.